MXene/graphitic carbon nitride-supported metal selenide for all-solid-state flexible supercapacitor and oxygen evolution reaction

Shrabani De[a], Jose Florentino[b], Gayani Pathiraja[c], Bhoj Raj Gautam[b], Bishnu Prasad Bastakoti[a*]

[a]Department of Chemistry, North Carolina A&T State University,1601 E. Market St. Greensboro, NC 27411 (USA)

[b]Department of Chemistry, Physics, and Materials Science, Fayetteville State University, 1200 Murchison Road, Fayetteville, NC 28301 (USA)

[c]Department of Nanoscience, Joint School of Nanoscience and Nanoengineering, University of North Carolina at Greensboro, 2907 East Gate City Blvd, Greensboro, NC 27401 (USA)

*Email: bpbastakoti@ncat.edu

S1. Experimental Section

Preparation of gel electrolyte (PVA-KOH)

The PVA-KOH gel electrolyte was prepared following the previously reported method[1]. Typically, 20 ml 9 wt% PVA solution was first prepared at 90 °C. Then, 10 ml KOH solution (10 wt%) was added dropwise into the PVA solution. The obtained semi-transparent liquid was used as gel electrolyte for the fabrication of flexible device.

Electrochemical measurements for supercapacitor

All electrochemical analyses, including three-electrode and two-electrode setup, were performed on a BioLogic VSP-50 electrochemical workstation. The electrochemical performance in three-electrode configuration was analyzed in 1 M KOH electrolyte. Electroactive material coated graphite rod was used as working electrode with Ag/AgCl electrode and Pt wire, serving as reference and counter electrodes, respectively. The working electrode was prepared by drop-casting a slurry of electroactive materials (by mixing the prepared samples (80 wt%), carbon black (10 wt%), and PVDF (10 wt%) with few drops of NMP) on a flat surface of an acid-cleaned graphite rod. Cyclic voltammetry (CV) and the galvanostatic charging discharging (GCD) study were carried out within a potential range of 0.0 to 0.5 V to evaluate the electroactivity of the prepared samples. The mass loading of active material was 0.25 mg. The electrochemical impedance spectroscopy (EIS) analysis was

conducted from a frequency of 1 MHz to 1 Hz at 10 mV amplitude at room temperature. The specific capacitance (C in F g^{-1}) was evaluated using GCD plots by using the Eq. S1[2]:

$$C = \frac{i \times \Delta t}{m \times \Delta V} \quad \text{.....S1}$$

Where, i is the charging–discharging current, Δt is the time required in seconds for the discharge cycle, m is the mass loaded, and ΔV is the voltage range.

The specific capacitance (C in F g^{-1}) of the device was calculated using Eq. S2[2]. The specific energy density (E in W h kg^{-1}) and power density (P in W kg^{-1}) of the device were evaluated using Eq. S3, and Eq. S4, respectively[2]:

$$C = \frac{2 \times i \times \Delta t}{m \times \Delta V} \quad \text{.....S2}$$

$$E = \frac{C\Delta V^2}{7.2} \quad \text{.....S3}$$

$$P = \frac{E \times 3600}{\Delta t} \quad \text{.....S4}$$

The stored charge (Q) is dependent on specific capacitance (C), voltage window (ΔV), and mass of the active material (m) of the corresponding electrode[3].

$Q = C \times \Delta V \times m$ S5

When the charge equivalence ($Q_+ = Q_-$) is applied, the mass ratio (m_+/m_-) of the positive and negative electrode can be calculated using the following equation[3]:

$$\frac{m_+}{m_-} = \frac{C_- \Delta V_-}{C_+ \Delta V_+} \quad \text{.....S6}$$

The calculated mass ratio of positive and negative electrode using Eq. S6 is 0.2.

The volumetric energy density of the all-solid-state asymmetric supercapacitor (ASSASC) device was also evaluated using the following method. The specific energy density (E) was calculated from the discharge time obtained from the GCD analysis using Eq. S3. The dimension of the current collector (carbon cloth) was 2 cm × 2 cm × 0.04 cm.

The volumetric energy density (E_v) could be estimated by Eq. S7[4]:

$$E_v = \frac{E \times m}{2 \times 2\ cm \times 2\ cm \times 0.04\ cm} \quad \text{.....S7}$$

Where, 'm' is the sum of the active masses (in kg) of the positive electrode (MCN/CESe-5:1) and negative electrode (MXene). The active masses of positive and negative electrode for the ASSASC device were 3.5 mg and 17 mg, respectively. The volume of two pieces of current collectors as negative electrode and positive electrode is $2 \times 2\ cm \times 2\ cm \times 0.04\ cm$.

Electrochemical measurements for oxygen evolution reaction (OER)

The OER study was performed using nanomaterial-modified glassy carbon electrodes (GCE) as a working electrode. The GCE was 3 mm diameter. The electrode was cleaned with alumina slurry for 2 minutes and then washed with water several times and dried in oven. The cleaned GCE was coated by drop casting of the nanomaterial ink and dried in oven at 60 °C. Slurry of the electroactive material was prepared following the same method as supercapacitor study. Pt wire and Ag/AgCl electrode were used as counter and reference electrode, respectively.

The electrochemical properties of the synthesized nanomaterials for OER were performed in three electrode electrochemical setup using 1 M KOH (pH=14) solution as electrolyte and the scan rate was kept at 20 mV s^{-1}. The methods used to study the electrochemical properties of the materials were linear sweep voltammetry (LSV), and chronoamperometry. The potentials of the electrode materials were determined by taking reversible hydrogen electrode (RHE) as the reference. The equation of the electrode potential with respect to RHE is given by:

$$E_{RHE} = E^{\circ}_{Ag/AgCl} + 0.059 \times pH + E_{Ag/AgCl} \quad \text{.....S8}$$

where, $E^{\circ}_{Ag/AgCl}$ (0.197 V) is the standard reduction potential of Ag/AgCl electrode at 25 °C and $E_{Ag/AgCl}$ is the electrode potential of the nanomaterial-coated-GCE with reference to Ag/AgCl. The coated and exposed geometrical surface area of each of the electrodes was calculated to be 0.071 cm^2. Since, 1 M KOH (pH=14) solution was used as a supporting electrolyte for study of OER on the prepared materials,

therefore, $E_{RHE} = (1.023 + E_{Ag/AgCl})\ V$ S9

Another method of studying the OER activities of the prepared electrocatalysts, is graphing Tafel plots according to the following Tafel equation[5]:

$$\eta = a + \frac{2.303RT}{\alpha nF}\log_{10}(j) \quad \text{.....S10}$$

The plot has a slope of $\frac{2.303RT}{\alpha nF}$, where R is the universal gas constant, T is the temperature in kelvin (K), α is the transfer coefficient, n is the number of electrons transferred in a redox half-cell, F is the Faraday constant (= 96500 C) and a is a constant.

The overpotential (η) is calculated by subtracting the water splitting potential (1.23 V) from the working electrode potential, i.e.,

$$\eta = (E_{RHE} - 1.23)\ V \quad \text{.....S11}$$

The Tafel slope is an important factor to understand the electrocatalytic activity of the prepared material, which is determined from electrochemical reaction mechanism. In the present work, the Tafel slope has been determined from the linear portion of the polarization curve.

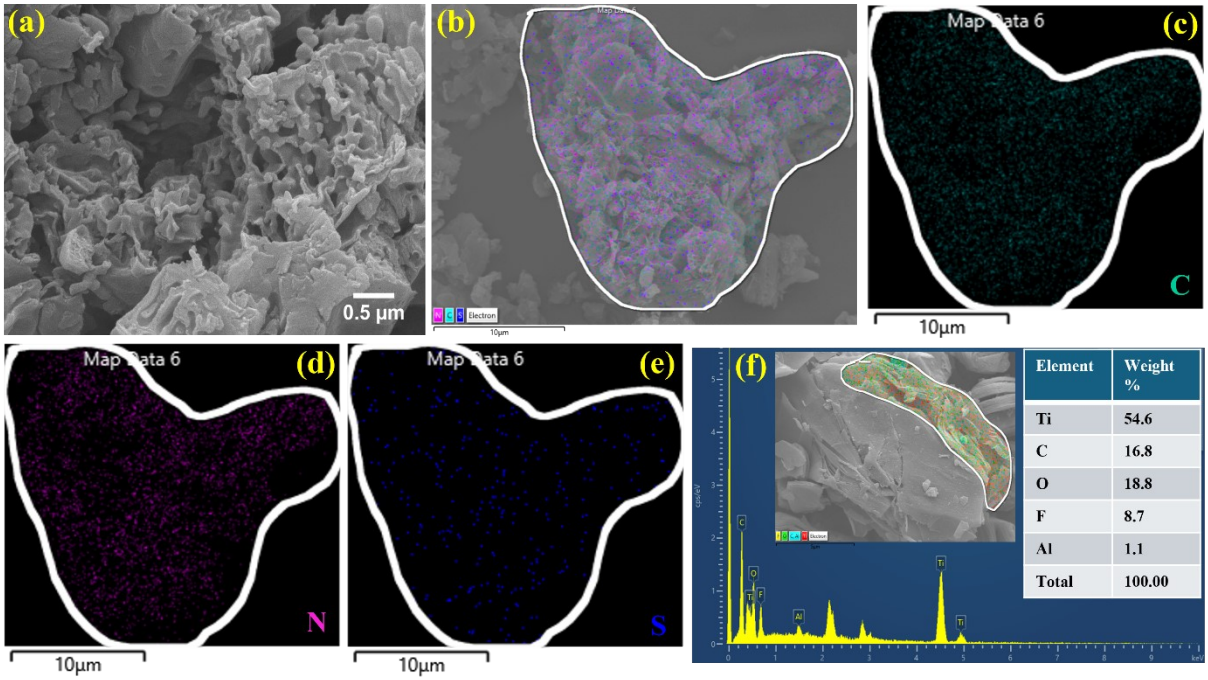

Fig. S1 (a) FESEM image of S-CN, (b) elemental mapping overlay area, (c-e) elemental mapping of C, N, and S, respectively of S-CN, (f) EDS analysis of $Ti_3C_2T_x$ with percentage of different elements present.

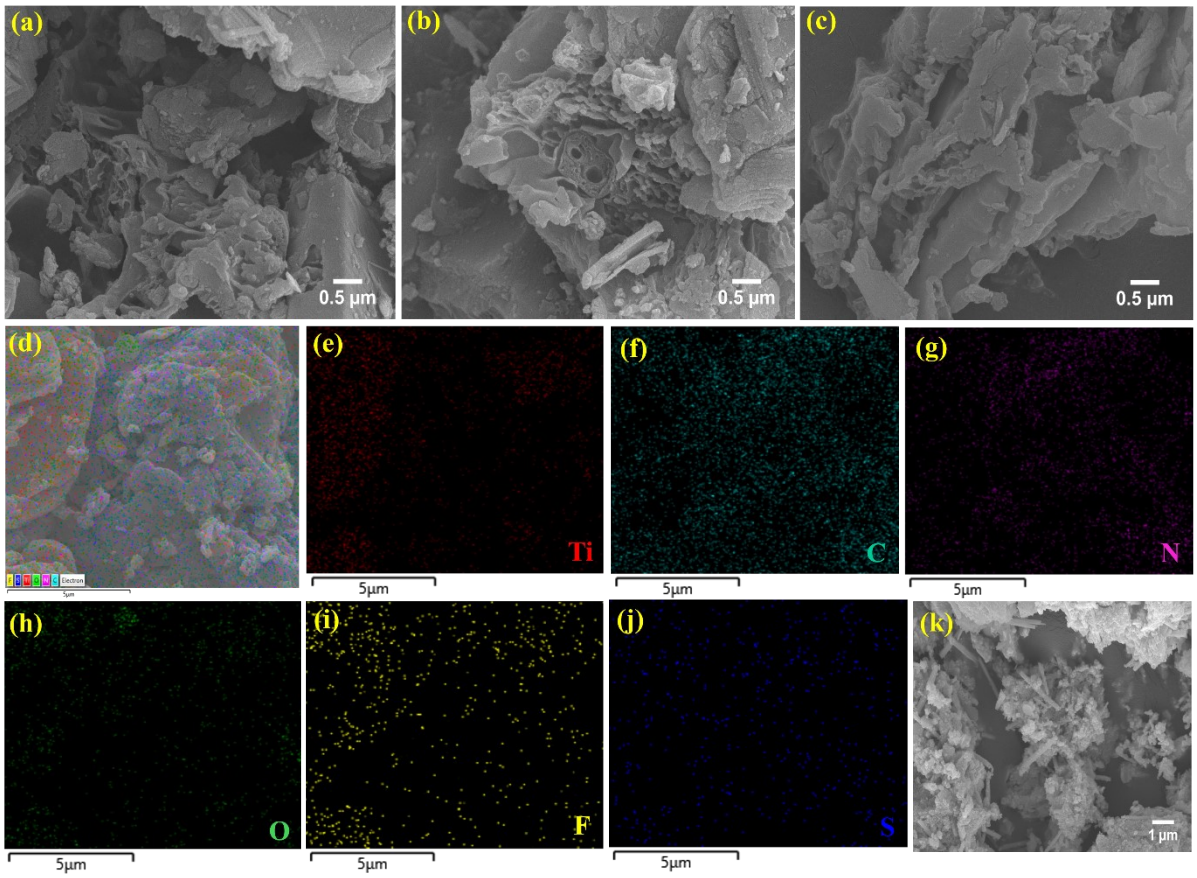

Fig. S2 FESEM images of (a) MCN-2:1, (b) MCN-4:1, (c) MCN-8:1, (d) elemental mapping overlay area of MCN-4:1, (e-j) elemental mapping of Ti, C, N, O, F, and S, respectively, (k) FESEM image of CESe.

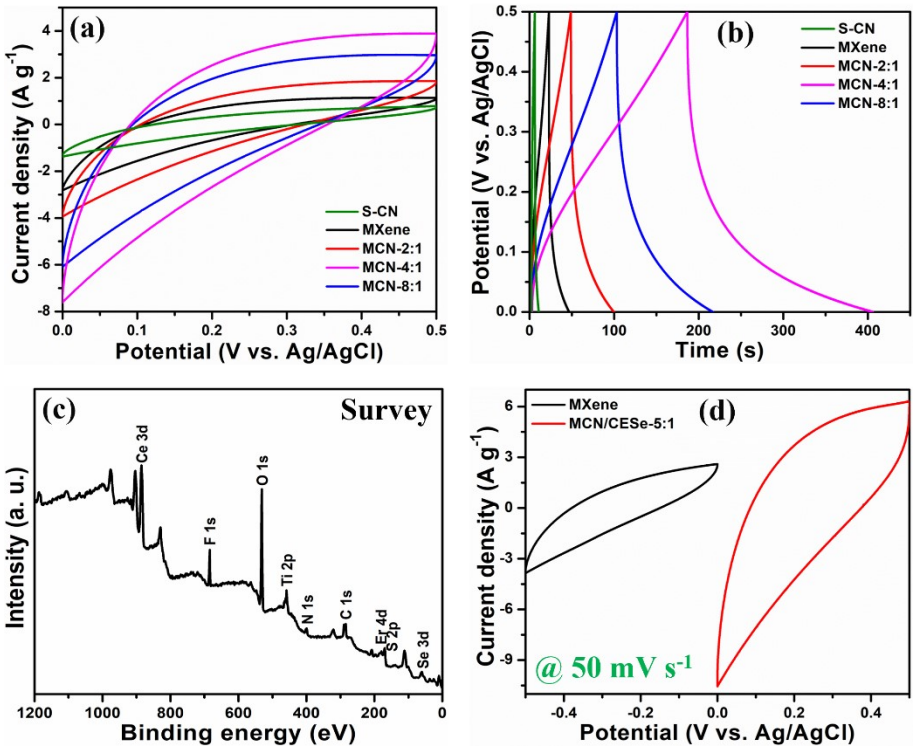

Fig. S3 Three-electrode electrochemical analysis comparison of S-CN, MXene, MCN-2:1, MCN-4:1, and MCN-8:1 (a) CV, and (b) GCD comparison, (c) XPS survey analysis of MCN/CESe-5:1, and (d) CV comparison of positive electrode MCN/CESe-5:1 and negative electrode MXene at 50 mV s^{-1} scan rate in three-electrode set-up.

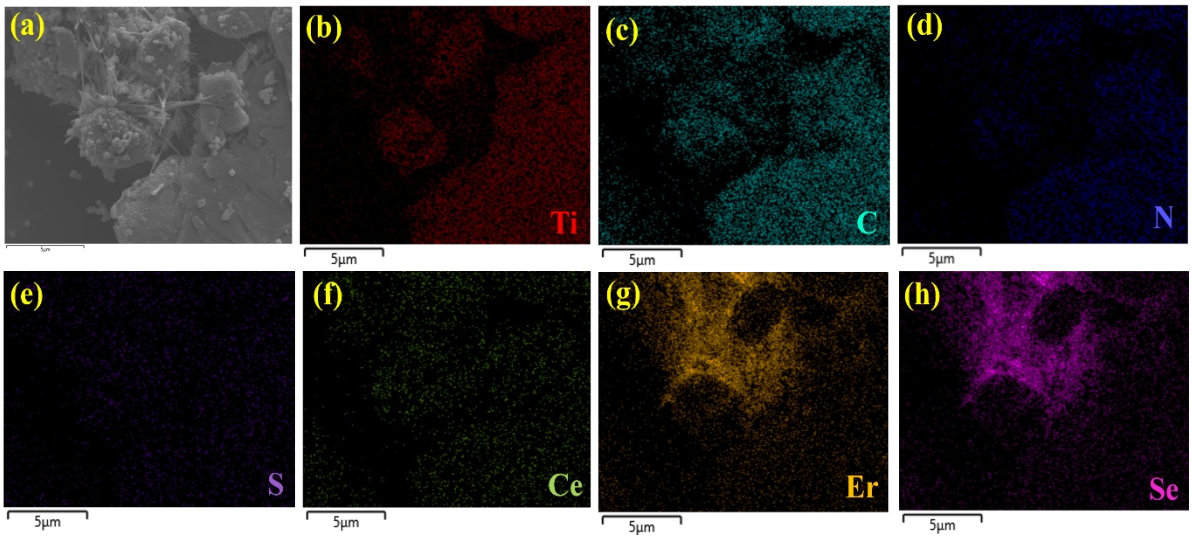

Fig. S4 (a) FESEM elemental mapping area, and (b-h) elemental mapping of Ti, C, N, S, Ce, Er, and Se, respectively of MCN/CESe-5:1.

Table S1. Fitted values of Nyquist impedance plot for three electrode analysis.

Synthesized composites	**R_{ESR} (Ω)**
MCN-4:1	1.067
MCN/CESe-3:1	0.921
MCN/CESe-5:1	0.565
MCN/CESe-7:1	1.1

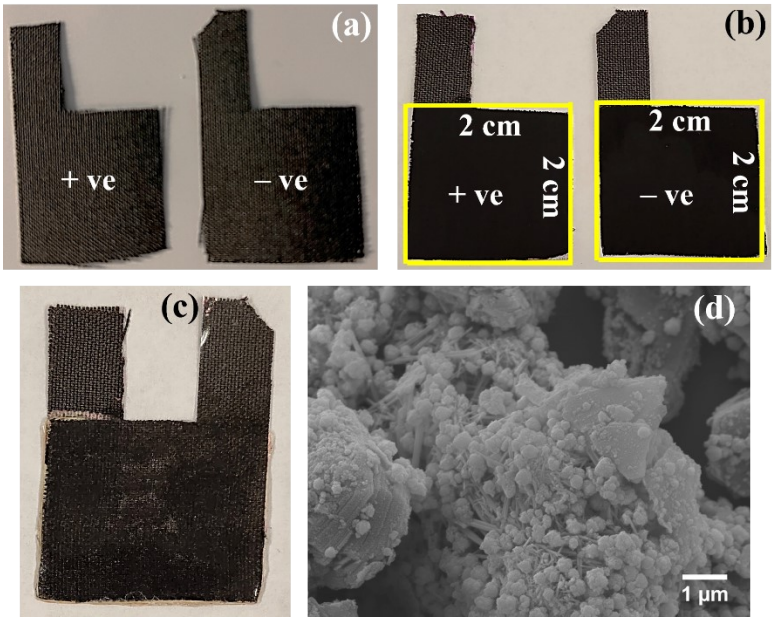

Fig. S5 Digital photograph of (a) bare carbon cloth (current collector), (b) electroactive material coated carbon cloth, (c) assembled flexible ASSASC device; (d) FESEM image of MCN/CESe-5:1 after the cyclic stability study.

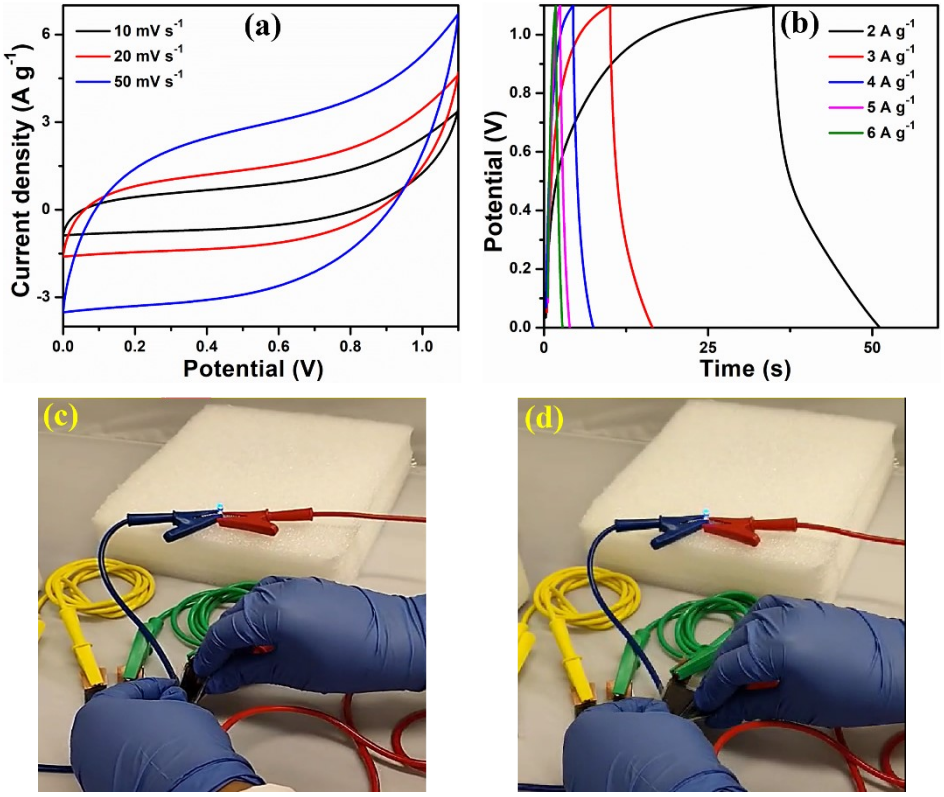

Fig. S6 (a) CV, and (b) GCD profiles of ASSASC device, (c, d) photograph showing flexibility of the assembled ASSASC device.

Table S2. Comparison of two electrode performances of fabricated ASSASC device with few previously reported $Ti_3C_2T_x$-based devices.

$Ti_3C_2T_x$-based device (+//-)	**3E**	**2E**							**Ref.**
	C (F g^{-1})	**Electrolyte**	**C (F g^{-1})**	**ED (Wh kg^{-1})**	**PD (W kg^{-1})**	**Current density**	**% of Sp.C retention**	**No. of cycles**	
$Ti_3C_2T_x$/NCF// $Ti_3C_2T_x$/NCF	332 at 0.5 A g^{-1}	PVA/KOH	63	8.75	1871	1 A g^{-1}	96	2500	6
$Ti_3C_2T_x$//AC	118 at 1 A g^{-1}	PVA/Li_2SO_4	46	5.5	500	25 mV s^{-1}	98	3000	7
rGO//$Ti_3C_2T_x$	-	1M H_2SO_4	48	8	50	2 mV s^{-1}	76	1000	8
MXene/CNT// MXene	550 at 2 mV s^{-1}	PVA/H_2SO_4	53	7.34	50	0.1 A g^{-1}	99	5000	9
MXene/rGO// MXene/rGO	397 at 0.5 A g^{-1}	PVA/H_2SO_4	65	3.81	163	0.5 A g^{-1}	94.5	10,000	10
$Ti_3C_2T_x$-Ar//$Ti_3C_2T_x$-Ar	212 at 1 A g^{-1}	KOH (30 wt%)	77.5	5.43	700	10 mV s^{-1}	94.8	10,000	11
MXene/MPFs/ /MXene/MPFs	326 at 0.1 A g^{-1}	PVA/H_2SO_4	40.7	2.04	601.5	0.01 A g^{-1}	95.9	7000	12
N-$Ti_3C_2T_x$//N-$Ti_3C_2T_x$	449 at 2	PVA/H_2SO_4	70	9.57	250	5 mV s^{-1}	79.6	2000	13

	mV s^{-1}								
CoS@MXene/CF//AC	250 at 1 A g^{-1}	PVA/KOH	41.5	10.66	678.1	0.2 A g^{-1}	96.87	5000	[14]
$Ti_3C_2T_x$//$Ti_3C_2T_x$	372 at 1 A g^{-1}	PVA/H_2SO_4	151	4.7	242	0.5 A g^{-1}	85	4000	[15]
MXene/N-$CuMe_2Pc$//MXene/N-$CuMe_2Pc$	786 at 0.5 A g^{-1}	1M H_2SO_4	~60 at 2 A g^{-1}	8.84	112.3	0.5 A g^{-1}	92.3	20,000	[16]
f-MXene//f-MXene	341 at 1 A g^{-1}	3M H_2SO_4	83	6.1	175	1 A g^{-1}	89.3	10,000	[17]
MCN/CESe-5:1//$Ti_3C_2T_x$	973	PVA/KOH	60	10.1	2203.6	2 A g^{-1}	100	10,000	**This work**

*NCF-N-doped carbon foam; AC-activated carbon; CNT-carbon nanotube; rGO-reduced graphene oxide; MPFs-metal porphyrin frameworks; CF-carbon foam; N-$CuMe_2Pc$-non-peripheral octamethyl-substituted copper (II) phthalocyanine; f-MXene-freeze-dried MXene.

Table S3. Comparison of electrocatalytic activity with some previously reported electrode materials.

Electrocatalyst	**Electrolyte**	**Overpotential (η_{10}) (mV)**	**Tafel slope (mV dec^{-1})**	**Ref.**
Co_3O_4/Ti_3C_2	1 M KOH	300	118	[18]
$CuCo_2O_4/Ti_3C_2$/NF	1 M KOH	360	49	[19]
V_2C	0.1 M KOH	430	68	[20]
Nb-MXene	1 M KOH	460	161	[21]
$MoSe_2$/MXene	1 M KOH	340	90	[22]
NiMn-LDHs/Ti_3C_2	1 M KOH	294	83.7	[23]
FeOOH NSs/Ti_3C_2	1 M KOH	400	95	[24]
MXene/NiCo-LDHs	0.5 M H_2SO_4	300	140	[25]

MCN/CESe-5:1	**1 M KOH**	**280**	**99**	**This work**

*NF-Nickel foam; LDHs-layered double hydroxides; NSs-nanosheets.

S2. Calculation of electrochemical double layer capacitance (C_{dl}) and electrochemically active surface area (ECSA)

Cyclic voltammetry (CV) analysis was performed in the non-Faradaic region to evaluate electrochemically active surface area (ECSA) of the synthesized electrocatalysts. This surface area is proportional to the electrochemical double layer capacitance (C_{dl}) of the solid-liquid interface[26, 27]. Fig. S7(b-f) show the CV curves recorded in 1 M KOH within the potential range of 0.923 to 1.123 V vs. RHE in different scan rates such as 20, 60, 100, 140, 180, and 220 mV/s. At the center of the potential range (1.025 V vs. RHE), the difference in current density (Δ j) between the anodic (j_a) and cathodic (j_c) current densities was calculated for each scan rate. By plotting Δ j against scan rate (V), the double layer capacitance (C_{dl}) was determined. The value of C_{dl} can be calculated from the slop of this linear fitting diagram according to the following Eq. (S12)[5].

$$C_{dl} = \frac{\Delta j}{V} \quad \text{……..S12}$$

ECSA of the electrocatalysts was calculated used following Eq. S13[5].

$$\text{ECSA} = \frac{C_{dl}}{C_s} \quad \text{……..S13}$$

Here, the standard specific capacitance (C_s) of a surface with 1 cm^2 surface area have the value of 0.04 mF cm^{-2}[28].

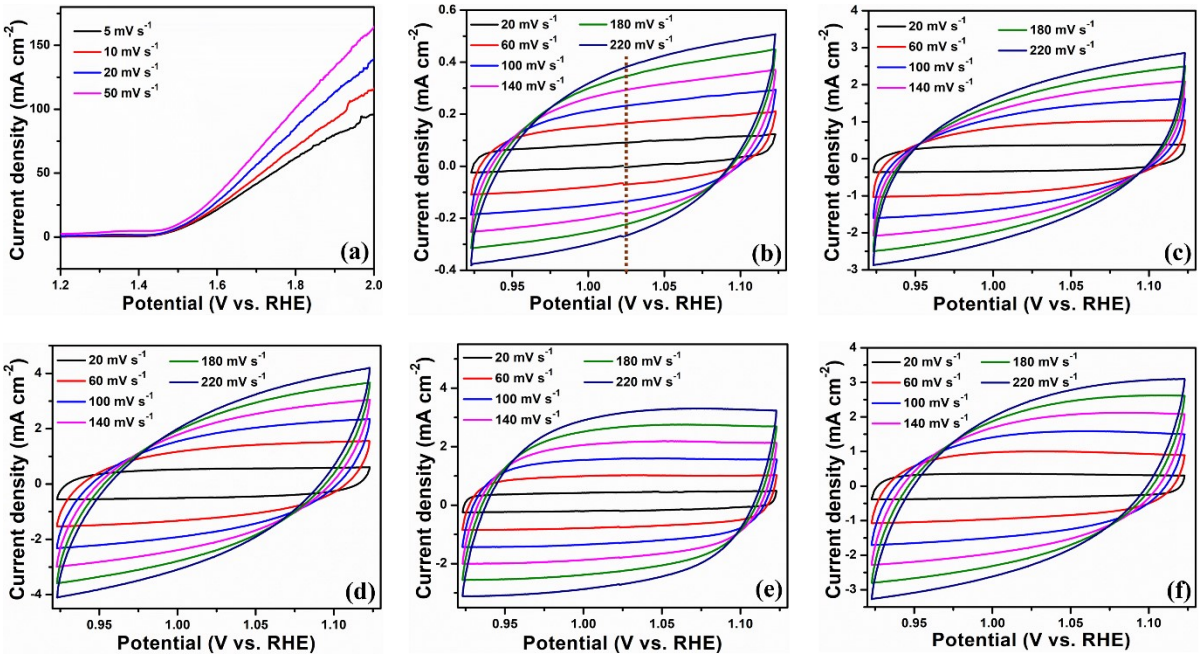

Fig. S7 (a) LSV profiles of MCN/CESe-5:1 in different scan rates; electrochemical double layer capacitance measurement using CV analysis at different scan rates within the voltage window of 0.923 to 1.123 V vs. RHE in 1 M KOH of (a) MXene, (b) MCN-4:1, (c) MCN/CESe-3:1, (d) MCN/CESe-5:1, and (e) MCN/CESe-7:1.

Table S4. Electrochemical double-layer capacitance (C_{dl}) and electrochemically active surface area (ECSA) values of synthesized materials.

Synthesized Materials	C_{dl} (mF cm^{-2})	ECSA (cm^2)
MXene	2.78	69.5
MCN-4:1	15.2	380
MCN/CESe-3:1	21.14	528.5
MCN/CESe-5:1	26.22	655.5
MCN/CESe-7:1	20.34	508.5

S3. Calculation of turn over frequency (TOF)

The turnover frequency (TOF) is used to measure the intrinsic OER efficiency. The number of active sites (n) must be determined to calculate the TOF value, and this information is obtained by running a CV in 1 M KOH in the range of 0.0-1.0 V at a scan rate of 20 mV s^{-1}. The number of active sites and overall charge of the electrocatalysts were determined using the following equations[29].

$$Q = \frac{\int_{E1}^{E2} IdE}{V} \quad \text{……..S14}$$

$$n = \frac{Q}{4F} \quad \text{……..S15}$$

Here, E is potential, Q is charge, and *V* is scan rate. Per-site turnover frequencies (TOF in s^{-1}) can be estimated by substituting the value of 'n' in the following Eq. (S16)[29].

$$TOF = \frac{I}{4nF} \quad \text{……..S16}$$

I = Current (in A) during the linear sweep measurement at certain overpotential (300 mV).

F = Faraday constant (96485 C mol^{-1}).

n = Number of active sites (in mol).

Four electrons are needed to create one oxygen molecule, as shown by the factor 1/4 in Eq. (S15, S16).

References

1. S. De, S. Acharya, S. Sahoo and G. C. Nayak, *Energy Advances*, 2024, **3**, 774-777.
2. S. De, C. K. Maity, S. Sahoo and G. C. Nayak, *ACS Applied Energy Materials*, 2021, **4**, 3712-3723.
3. E. Redondo, L. W. Le Fevre, R. Fields, R. Todd, A. J. Forsyth and R. A. Dryfe, *Electrochimica Acta*, 2020, **360**, 136957.
4. S. De, C. K. Maity, M. J. Kim and G. C. Nayak, *Electrochimica Acta*, 2023, **463**, 142811.
5. S. De, S. Roy and G. C. Nayak, *Materials Today Nano*, 2023, **22**, 100337.
6. L. Sun, G. Song, Y. Sun, Q. Fu and C. Pan, *ACS Applied Materials Interfaces*, 2020, **12**, 44777-44788.
7. T.-H. Chang, T. Zhang, H. Yang, K. Li, Y. Tian, J. Y. Lee and P.-Y. Chen, *ACS Nano*, 2018, **12**, 8048-8059.
8. A. M. Navarro-Suárez, K. L. Van Aken, T. Mathis, T. Makaryan, J. Yan, J. Carretero-González, T. Rojo and Y. Gogotsi, *Electrochimica Acta*, 2018, **259**, 752-761.
9. X. Shi, F. Guo, K. Hou, G. Guan, L. Lu, Y. Zhang, J. Xu and Y. Shang, *Energy & Fuels*, 2023, **37**, 9704-9712.
10. D. Jiang, J. Zhang, S. Qin, Z. Wang, K. A. S. Usman, D. Hegh, J. Liu, W. Lei and J. M. Razal, *ACS Nano*, 2021, **15**, 5000-5010.
11. R. B. Rakhi, B. Ahmed, D. Anjum and H. N. Alshareef, *ACS Applied Materials Interfaces*, 2016, **8**, 18806-18814.
12. W. Zhao, J. Peng, W. Wang, B. Jin, T. Chen, S. Liu, Q. Zhao and W. Huang, *Small*, 2019, **15**, 1901351.
13. M. Cai, X. Wei, H. Huang, F. Yuan, C. Li, S. Xu, X. Liang, W. Zhou and J. Guo, *Chemical Engineering Journal*, 2023, **458**, 141338.
14. L. Liao, A. Zhang, K. Zheng, R. Liu, Y. Cheng, L. Wang, A. Li and J. Liu, *ACS Applied Materials Interfaces*, 2021, **13**, 28222-28230.
15. X. Zhang, Y. Liu, S. Dong, J. Yang and X. Liu, *Journal of Alloys Compounds*, 2019, **790**, 517-523.
16. R. Ramachandran, Q. Hu, K. Rajavel, P. Zhu, C. Zhao, F. Wang and Z.-X. Xu, *Journal of Power Sources*, 2020, **471**, 228472.
17. F. Ran, T. Wang, S. Chen, Y. Liu and L. Shao, *Applied Surface Science*, 2020, **511**, 145627.
18. Y. Lu, D. Fan, Z. Chen, W. Xiao, C. Cao and X. Yang, *Science Bulletin*, 2020, **65**, 460-466.
19. S. Ghorbanzadeh, S. Hosseini and M. Alishahi, *Journal of Alloys Compounds*, 2022, **920**, 165811.
20. G. Kiran, T. Sreekanth, K. Yoo and J. Kim, *Materials Chemistry Physics*, 2023, **296**, 127272.
21. M. Gandara, M. N. de Arruda, J. M. K. Assis, M. d. J. O. Martins, L. Rakočević, D. Mladenović, B. Šljukić and E. S. Gonçalves, *Applied Materials Today*, 2024, **40**, 102356.
22. N. Li, Y. Zhang, M. Jia, X. Lv, X. Li, R. Li, X. Ding, Y.-Z. Zheng and X. Tao, *Electrochimica Acta*, 2019, **326**, 134976.
23. Y. Liu, L. Bai, T. Li, H. Liu, X. Wang, L. Zhang, X. Hao, C. He and S. Guo, *Materials Advances*, 2022, **3**, 4359-4368.
24. K. Zhao, X. Ma, S. Lin, Z. Xu and L. Li, *ChemistrySelect*, 2020, **5**, 1890-1895.
25. A. K. Sharma, V. Sharma, A. Debnath, V. Saxena and A. Mahajan, *Journal of Alloys Compounds*, 2023, **939**, 168779.
26. M. A. R. Anjum, M. H. Lee and J. S. Lee, *ACS Catalysis*, 2018, **8**, 8296-8305.
27. F. Meng, E. Hu, L. Zhang, K. Sasaki, J. T. Muckerman and E. Fujita, *Journal of Materials Chemistry A*, 2015, **3**, 18572-18577.
28. P. Connor, J. Schuch, B. Kaiser and W. Jaegermann, *Zeitschrift für Physikalische Chemie*, 2020, **234**, 979-994.

29. H. Deng, C. Zhang, Y. Xie, T. Tumlin, L. Giri, S. P. Karna and J. Lin, *Journal of Materials Chemistry A*, 2016, **4**, 6824-6830.